Organic Salts as a Route to Energy Level Control in Low Bandgap, High Open-Circuit Voltage Organic and Transparent Solar Cells that Approach the Excitonic Voltage Limit

*John Suddard-Bangsund, Christopher J. Traverse, Margaret Young, Tyler J. Patrick, Yimu Zhao, and Richard R. Lunt**

A new series of organic salts with selective near-infrared (NIR) harvesting to 950 nm is reported, and anion selection and blending is demonstrated to allow for fine tuning of the open-circuit voltage. Extending photoresponse deeper into the NIR is a significant challenge facing small molecule organic photovoltaics, and recent demonstrations have been limited by open-circuit voltages much lower than the theoretical and practical limits. This work presents molecular design strategies that enable facile tuning of energy level alignment and open-circuit voltages in organic salt-based photovoltaics. Anions are also shown to have a strong influence on exciton diffusion length. These insights provide a clear route toward achieving high efficiency transparent and panchromatic photovoltaics, and open up design opportunities to rapidly tailor molecules for new donor–acceptor systems.

1. Introduction

Organic photovoltaics (OPVs) are approaching commercial viability due to their potential for inexpensive, high-throughput manufacturing, and unique applications, such as flexible and transparent solar cells. However, few small molecule organic photovoltaics have been demonstrated with efficient photoconversion into the deep near-infrared (NIR), leaving almost half the incident solar photon flux unutilized.[1] Modest photoresponse up to 1600 nm has been shown in porphyrin tape and carbon nanotube based photodetectors,[2,3] and efficiencies near 1% have been shown in carbon nanotube photovoltaics with photoresponse to 1200 nm.[4] In part, the development of efficient NIR OPVs is complicated by their small bandgaps and the inherent trade-off between the achieving a high V_{OC}, by maximizing the interface gap, and efficiently dissociating excitons, by maximizing donor–acceptor lowest unoccupied molecular orbitals (LUMO) offset energies. With smaller bandgaps, it thus becomes more challenging to identify suitable acceptor pairings due to the heightened tolerance for optimal energy level alignment. For example, tin phthalocyanine (SnPc) and lead phthalocyanine (PbPc), which both have absorption cut-offs near 1000 nm, exhibit V_{OC}'s of only 0.42 and 0.47 V, respectively, under 1 sun illumination,[5,6] nearly half of the realistic excitonic voltage limit.[7] Because of this voltage limitation and limited spectral coverage, current demonstrations of transparent organic photovoltaics (TPVs) with high transparency have been limited to 2%–4%.[8,9] To address this challenge and expand the catalog of efficient selectively NIR harvesting molecules, we demonstrate a molecular design technique for sensitive energy level control to allow for the rapid realization of novel donor–acceptor pairings with both efficient NIR response and high voltage near the excitonic limit. This demonstration can ultimately enhance the performance of panchromatic tandem cells, and single- and multi-junction transparent photovoltaics.

Polymethines, or cyanines (Cy), are a highly promising class of molecules that can satisfy the need for efficient, NIR-selective harvesting for transparent photovoltaics. They are a class of ionic organic salts that have gained research attention for applications in photodetectors,[10] all-optical switching,[11] transparent luminescent concentrators,[12] and photovoltaic applications due to their versatile chemistry and outstanding photophysical properties.[13,14] Notably, polymethines feature tunable absorption, high extinction coefficients, high solubility, and suppressible oscillator strength in the visible part of the solar spectrum. Recently, polymethines with absorption in the near-infrared have been employed in OPV devices with efficiencies of 0.9%–2.8% for opaque devices and semitransparent devices.[15,16]

Despite these promising achievements, the performance of polymethine OPVs is still constrained by V_{OC}'s far below the

J. Suddard-Bangsund, C. J. Traverse, M. Young, T. J. Patrick, Dr. Y. Zhao, Prof. R. R. Lunt
Department of Chemical Engineering and Materials Science
Michigan State University
East Lansing, MI 48824, USA
E-mail: rlunt@msu.edu
Prof. R. R. Lunt
Department of Physics and Astronomy
Michigan State University
East Lansing, MI 48824, USA

DOI: 10.1002/aenm.201501659

realistic voltage limit. Current efforts to improve polymethine photovoltaics have focused on studying the influence of the conjugation and counterion chemistry of larger gap polymethine cores on device performance, optical properties, and solid state packing.[16–19] Notably, Véron et al. recently demonstrated that by exchanging PF_6^-, a small anion with relatively high electronegativity, for a bulky halogenated aromatic anion, V_{OC} and the short-circuit current density (J_{SC}) could be enhanced by nearly 50%.[16] However, little is currently understood about the energetic landscape of polymethines, the role of various anions, or the mechanisms behind such enhancements.

In this work, we systematically study the influence of the counterion on the photovoltaic performance of new heptamethine salts with deeper NIR-selective absorption to 950 nm. We demonstrate that both V_{OC} and the peak external quantum efficiency in the NIR can be enhanced by over 70% by exchanging traditional counterions such as I^- or PF_6^- with carefully selected bulky halogenated aromatic counterions. We further show that bulkiness alone is not the ultimate criteria, as differing bulky anions show significant variations in enhancement. We attribute these simultaneous improvements to frontier energy level shifts in the solid state and an increased interface gap, as well as enhancement in exciton diffusion length (L_D). Exploiting these effects, we find that the polymethine energy levels can be finely tuned by varying the composition of counterion mixtures, or alloying counterions, to control frontier energy level positions and subsequently interface gaps. These insights provide design tools for optimizing the energy level alignment of polymethines for various donor–acceptor systems, expand the possibility of efficient, high voltage organic photovoltaics for a range of applications with selective absorption deeper in the NIR, and highlight the key importance of bulky anion selection.

2. Results

We report the synthesis, characterization, and photovoltaic device performance of a series of new organic salts with selective absorption deeper in the NIR and high visible transparency. We focus on one new key NIR active heptamethine cation (Cy^+, shown in **Figure 1**) and systematically study the impact of varying counterion substitutions (see Figure 1a,b and Figure S1, Supporting Information) to demonstrate the potential for high performance opaque and transparent planar cells with NIR response past 900 nm. To improve the intrinsic comparability between various anions, each salt was prepared by a single-step solution-based counterion exchange from the same CyI parent compound. These counterions were chosen to systematically elucidate the effects of counterion size, electronegativity, and molecular structure on solid-state photophysical properties and device performance.

Figure 2 shows *J–V* characteristics of the most representative devices for each counterion under (a) 1 sun illumination and (b) dark conditions. The anion plays a dramatic role in *J–V* performance, where the V_{OC} is clearly enhanced from ≈0.4–0.45 V for CyI, $CyPF_6$, and $CySbF_6$ to 0.63 V for CyTRIS and 0.71 V for CyTPFB, all with nearly identical bandgaps (absorption edges). Fill factor (FF) is highest for CyTRIS at 0.62 and lowest for CyI at 0.32. A gradual increase is seen from $CyPF_6$ at 0.49, $CySbF_6$ at 0.52, and CyTPFB at 0.60 (see **Table 1**). J_{SC} is modestly increased following the V_{OC} trend.

The dark *J–V* curves were fit to the ideal diode equation,[20] to extract the series resistance, R_S, parallel resistance, R_P, dark ideality factor, n_{id}, and reverse dark saturation current, J_0, as fitting parameters. Fitting results are summarized in **Table 2**. R_P shows little variation across the five counterions, with the exception of

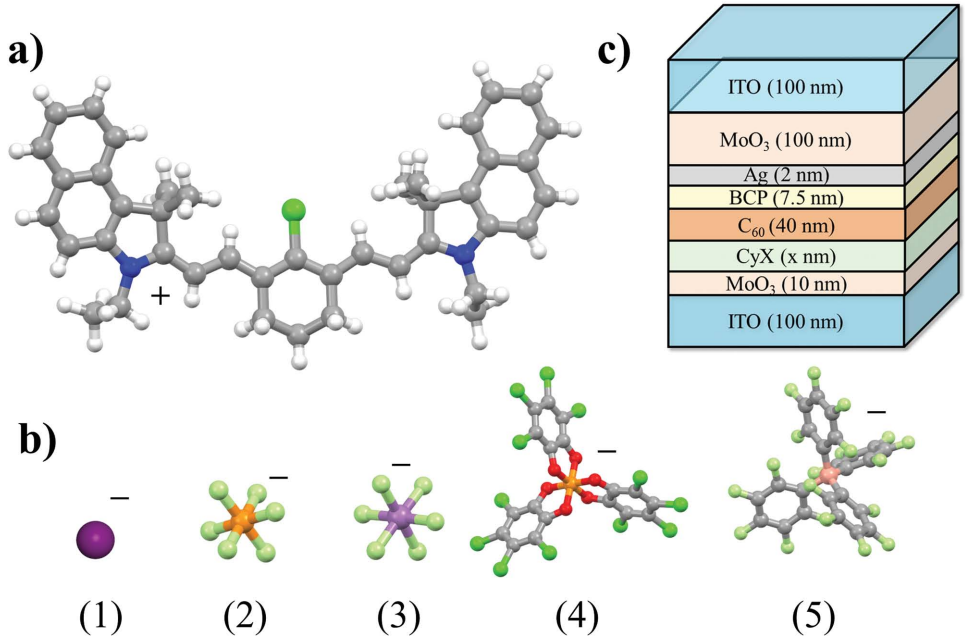

Figure 1. Molecular structures of a) the polymethine cation (Cy^+) and b) the counterions studied here: (1) I^-, (2) PF_6^-, (3) SbF_6^-, (4) Δ-tris(tetrachloro-1,2 benzenediolato)phosphate(V) (known as Δ-TRISPHAT$^-$, and further abbreviated as $TRIS^-$), and (5) Tetrakis(pentafluorophenyl)borate ($TPFB^-$). c) Typical device architecture. Opaque devices utilize a 100 nm thick Ag top cathode while transparent devices utilize a 2 nm Ag interfacial layer, a 100 nm MoO_3 protective capping layer, and a 100 nm thick ITO top cathode.

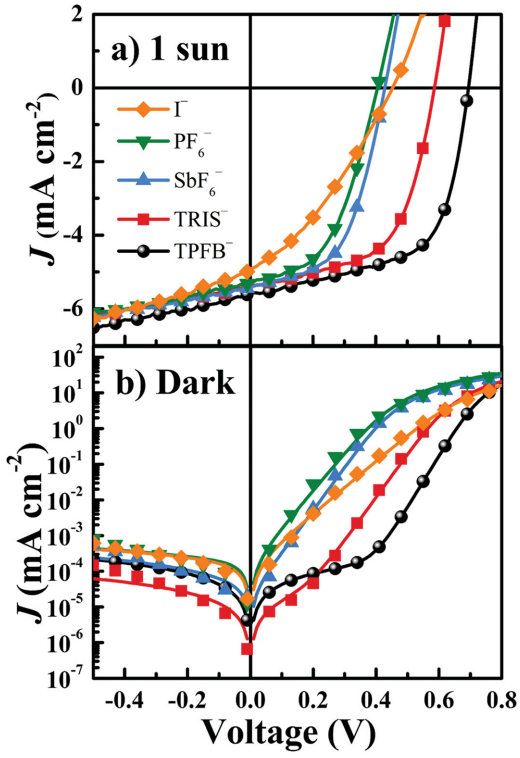

Figure 2. *J–V* curves for representative opaque devices for each counterion under a) 1 sun (nominal) illumination and b) dark conditions. Accounting for spectral mismatch, the equivalent illumination intensity ranged from 1.11 to 1.14 sun. The optimized opaque device structure for each counterion was ITO (100 nm)/MoO_3 (10 nm)/CyX (8–12 nm)/C_{60} (40 nm)/BCP (7.5 nm)/Ag (100 nm), where X is the anion highlighted in the legend.

$CySbF_6$, which shows a small possible enhancement in R_P. R_S similarly shows no clear dependence on counterion. The ideality factor is lowest for CyTPFB at n_{id} = 1.28, and highest for CyI, at n_{id} = 2.28. Typically, higher values of n_{id}, notably above n_{id} = 1.5, correspond to increases in trap-assisted recombination, for example, with an increase in the Urbach tail states.[21] Most significantly, J_0 is found to follow the trend in V_{OC} with differing anions, decreasing steadily from 1.3×10^{-7} mA cm^{-2} in CyI devices to 2.3×10^{-10} mA cm^{-2} in CyTPFB devices. This trend is consistent with the reduction of the recombination at the donor–acceptor interface from a larger interface gap that is implied by the ideal diode equation, and with other observations in literature.[5] However, while this data does not solely elucidate the mechanism of the voltage enhancement it does help to eliminate some mechanisms such as parallel shunting of ion conduction and is further clarified with anion alloying experiments.

Table 1. Average *J–V* characteristics for each counterion, X, in CyX illuminated under 1 sun nominal illumination. Accounting for spectral mismatch, *M*, the equivalent intensity ranges from 1.11 to 1.14 sun. The integrated J_{SC} is for the same intensity equivalent listed for each device.

Device	J_{SC} [mA cm^{-2}]	*M*	Int. J_{SC} [mA cm^{-2}]	V_{OC} [V]	FF	PCE [%]
$TPFB^-$	5.2 ± 0.5	1.11	4.7 ± 0.5	0.71 ± 0.01	0.60 ± 0.01	2.0 ± 0.2
$TRIS^-$	4.8 ± 0.5	1.12	4.4 ± 0.4	0.63 ± 0.01	0.62 ± 0.01	1.7 ± 0.2
SbF_6^-	5.1 ± 0.5	1.12	4.0 ± 0.4	0.43 ± 0.01	0.52 ± 0.01	1.0 ± 0.1
PF_6^-	5.0 ± 0.5	1.13	4.0 ± 0.4	0.40 ± 0.01	0.49 ± 0.01	0.9 ± 0.1
I^-	4.5 ± 0.5	1.14	3.5 ± 0.4	0.45 ± 0.01	0.32 ± 0.01	0.6 ± 0.1
Trans. $TPFB^-$	2.5 ± 0.3	1.12	1.7 ± 0.2	0.69 ± 0.01	0.53 ± 0.01	0.8 ± 0.1

Table 2. Fit ideal diode parameters for each counterion.

Anion	$n_{id,V}$[a]	n_{id}[b]	E_U[c] [meV]	R_P [MΩ cm^2]	R_S [Ω cm^2]	J_0 [mA cm^{-2}]
$TPFB^-$	1.17	1.28 ± 0.11	46	3.0 ± 0.8	4.8 ± 1.0	$(4.1 \pm 3.3) \times 10^{-12}$
$TRIS^-$	1.34	1.36 ± 0.01	55	19.2 ± 11.6	9.0 ± 1.8	$(1.3 \pm 0.2) \times 10^{-10}$
SbF_6^-	1.38	1.37 ± 0.01	56	6.8 ± 6.5	9.6 ± 0.2	$(1.6 \pm 0.3) \times 10^{-8}$
PF_6^-	1.34	1.58 ± 0.02	97	3.4 ± 1.9	8.6 ± 1.0	$(1.4 \pm 0.1) \times 10^{-7}$
I^-	1.18	2.28 ± 0.05	–[d]	1.1 ± 0.8	6.9 ± 0.8	$(1.4 \pm 0.2) \times 10^{-7}$

[a]Ideality factor fit from intensity dependent V_{OC} data; [b]Ideality factor fit from dark curves using the ideal diode equation; [c]The Urbach tail energy, calculated from the dark *J–V* ideality factor as $E_U = kT/(2n_{id}^{-1} = 1)$;[21] [d]Urbach tail energy cannot be calculated for n_{id} greater than 2.

Figure 3a shows the normalized extinction coefficients for each counterion. CyTPFB and CyTRIS show slightly narrower absorption widths compared to the other counterions, with absorption ranges of approximately 650–930 and 670–930 nm, respectively, compared to 620–950 nm for CyI, $CyPF_6$, and $CySbF_6$.

The external quantum efficiency (EQE) spectra in Figure 3b show enhanced photocurrent contribution from the polymethine donor in the CyTPFB and CyTRIS devices. EQE spectra (markers) were fit (solid lines) with a combined diffusion and optical interference model using least squares regression to extract donor and acceptor exciton diffusion lengths (L_D and L_A).[22] These enhancements correspond to an increase in exciton diffusion length, L_D, from 2.7 ± 0.8 nm in CyI to 5.0 ± 1.4 nm in CyTPFB (see **Table 3** and **Figure 4**b). Due to the concomitant increase in V_{OC}, FF, and L_D, the measured power conversion efficiency increases from 0.6% for CyI to 1.7% for CyTRIS and up to 2.0% for CyTPFB (see Table 1).

We note that the J_{SC} obtained by integrating the EQE with the AM1.5 solar spectrum, accounting for spectral mismatch, are about 10% lower than those measured directly under 1 sun (nominal) intensity. This discrepancy is due to the slight degradation due to testing in air without packaging and device-to-device variability (error propogation). We performed a limited lifetime test with packaged and unpackaged devices, and found that the EQE peak height typically drops by <10% within the first 30 min of testing for unpackaged devices (see Figure S2, Supporting Information) but is stable for >12 h thereafter.

In **Figure 5**, the intensity dependent *J–V* parameters are characterized for each counterion. Such intensity dependent data is useful for understanding the low-lighting performance and can provide additional insight into the recombination dynamics. At low intensities, CyI devices show recovery of FF. Other counterions show a nearly uniform FF, responsivity (J_{SC}/incident power), and PCE as a function of intensity, which makes the devices also promising for low lighting applications. The slopes of the V_{OC} versus intensity curves are comparable across all five counterions and can be fit to the intensity dependent ideality

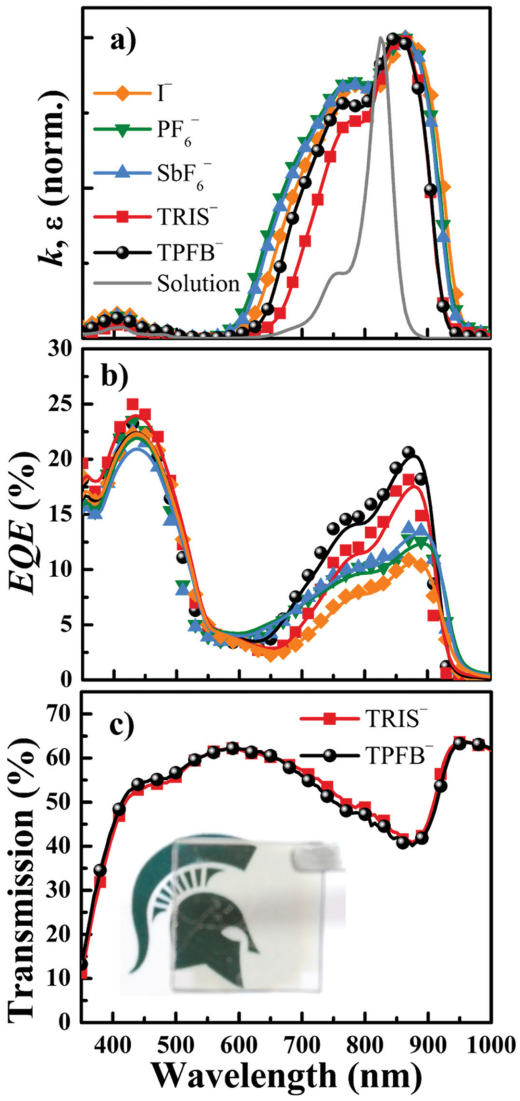

Figure 3. a) Normalized extinction coefficients for each organic salt and b) external quantum efficiency (EQE) of the optimized device structures for CyI, $CyPF_6$, $CySbF_6$, CyTRIS, and CyTPFB. c) Transmission scans of the full transparent devices for CyTRIS and CyTPFB. (Inset) Transparent solar cell device.

Table 3. Key device parameters and molecular properties for each cyanine-counterion pair.

Device	L_D [nm]	V_{OC} [V]	M_W [g mol^{-1}]	$r^{a)}$ [nm]	$n^{b)}$	E_g^{opt} [eV]	$\Delta E_{edge}^{c)}$ [eV]
$TPFB^-$	5.0 ± 1.4	0.71	768.6	0.463	2.24	1.34	−0.09
$TRIS^-$	4.5 ± 1.0	0.63	797.16	0.479	2.21	1.33	−0.09
SbF_6^-	2.7 ± 0.3	0.45	235.75	0.274	2.47	1.31	−0.11
PF_6^-	2.6 ± 0.2	0.41	144.96	0.266	2.49	1.31	−0.12
I^-	2.7 ± 0.8	0.45	126.9	0.197	2.76	1.30	−0.12

[a)]Equivalent spherical radius of the volume contained by the Connolly surface. Calculated with Materials Studio v7.0; [b)]The real index of refraction at the NIR peak (see Figure S17, Supporting Information); [c)]Energy difference between the low energy cut-off of the thin film and solution absorption spectra, determined at 5% of the peak height.

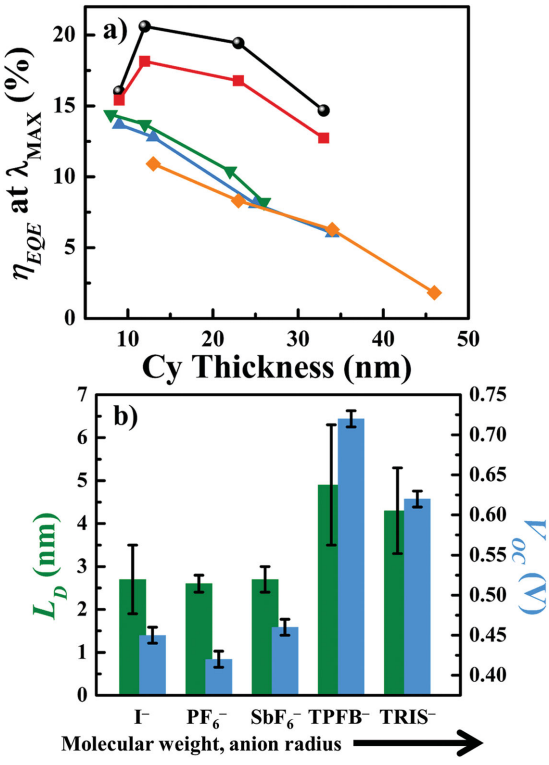

Figure 4. a) Thickness dependence of the peak EQE in the NIR for each counterion. CyTRIS and CyTPFB peak at a slightly higher thickness than the other counterions, likely due to a combination of lowered extinction coefficients and enhanced diffusion lengths (see Figure S17, Supporting Information). b) Exciton diffusion length (L_D), and V_{OC} for each counterion, ordered by increasing molecular weight and steric bulk and decreasing n index of refraction. This ordering was chosen to emphasize that there is no clear trend between any of these parameters.

factor, $n_{id,V}$, by assuming that R_P is much larger than R_S.[7] Values of $n_{id,V}$ range from 1.17 to 1.38 (see Table 2). CyTPFB shows the lowest $n_{id,V}$ of 1.17 (compared to n_{id} = 1.28), $CySbF_6$ shows the highest $n_{id,V}$ of 1.38 (compared to n_{id} = 1.37). While the $n_{id,V}$ values of $CySbF_6$, CyTRIS, and CyTPFB are comparable, and even within error of their fit dark ideality factors, the increased values of n_{id} seen in $CyPF_6$ and CyI (of 1.58 and 2.28, respectively) are not reflected in the intensity dependent fit $n_{id,V}$ (of 1.34 and 1.18, respectively). The differences in these extracted n_{id}'s and $n_{id,V}$'s stem from data collected in the dark versus the light, and is similar to many other organic and inorganic systems where diode parameters are found to vary under illumination. In all cases, $n_{id,V}$ is below 1.5, which suggests that trap-assisted recombination is less dominant and that a varying combination of both drift and trap-assisted recombination is likely present.[21,23]

To characterize exciton diffusion length, we measured EQE as a function of thickness for each counterion (see **Figure 6** and Figure S3, Supporting Information). CyTPFB and CyTRIS show significantly less EQE roll-off with increasing thickness, confirming an enhancement in the exciton diffusion length, charge collection length, or both. This trend can also be seen in Figure 4a, where the peak EQE is plotted as a function of thickness for each anion and follows the trend of fitted L_D enhancement (Figure 4b). Exciton diffusion lengths reported

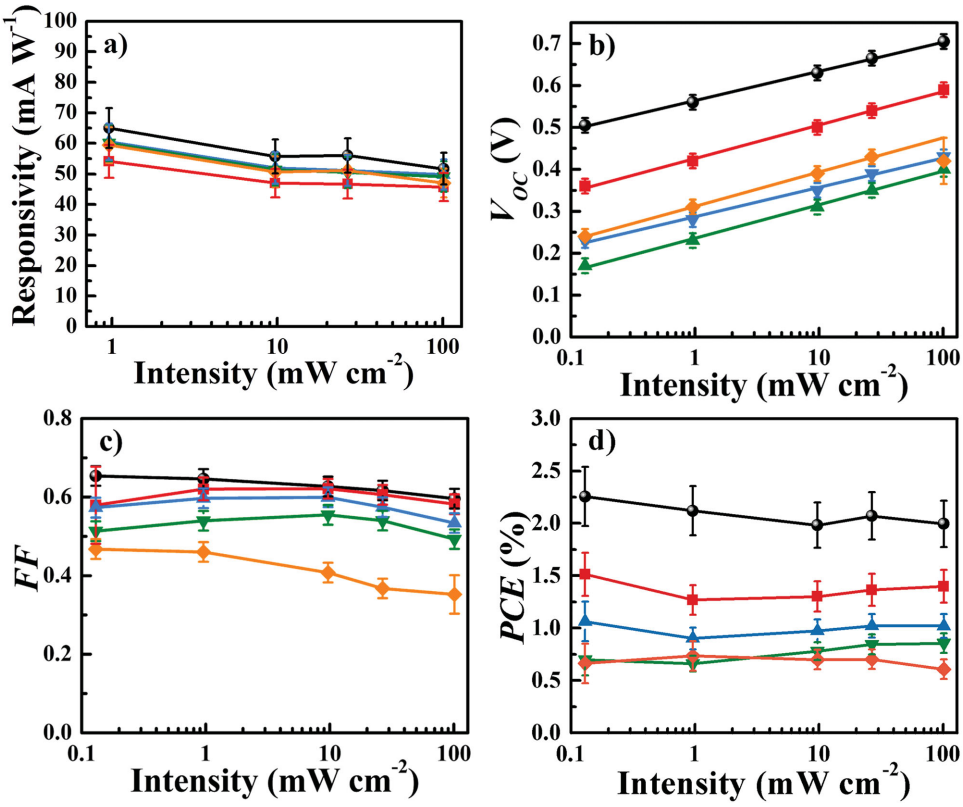

Figure 5. Intensity dependent *J–V* parameters for each counterion: a) Responsivity (J_{SC}/incident power), b) V_{OC}, c) FF, and d) PCE.

for each counterion in Table 3 are averaged across all thicknesses. In reality, the charge collection efficiency, η_{CC}, could diminish at larger thicknesses, thus suggesting that the diffusion lengths are likely lower estimates.

To demonstrate the potential of these molecules for efficient transparent PVs, we fabricated preliminary planar transparent devices with the architecture shown in Figure 1c with a 23 nm thick layer of CyTPFB. These planar devices showed an average PCE of 0.9%, with a J_{SC} of 2.5 ± 0.3 mA cm^{-2}, a V_{OC} of 0.69 V, and a FF of 0.53 (see Table 1), with an average visible transmittance (AVT) of 60.4% and a color rendering index (CRI) of 94.3. It is expected that the AVT and J_{SC} could be improved in these devices by further optimization of optical interference and blend formation for bulk heterojunction architectures. For example, the implementation of optical interference designs and NIR mirrors can nearly double J_{SC}, and antireflective coatings can add ≈8%, absolute, to the AVT.[8] A photo of the unpatterned CyTPFB transparent device grown concurrently with the devices is shown in the inset of Figure 3c. *J–V* and EQE (peak NIR EQE of 9% at 870 nm) for the most representative device can be found in Figure S4 of the Supporting Information.

3. Discussion

3.1. Open-Circuit Voltage Enhancement Via Energy Level Tuning

Open-circuit voltage enhancements are often understood by one of several mechanisms: (1) by a reduced leakage current, corresponding to better Ohmic contact at the electrodes;[5] (2) improved film quality and reduced pinholes or shunting;[24,25] (3) reduced mobile ion shunting;[26,27] (4) changes in the interface gap defined as the difference between the donor highest occupied molecular orbital (HOMO) and the acceptor LUMO; and (5) mid-gap trap states, either dilute or intrinsic, introduced by disorder, impurities, dark spin states (such as triplet states), or other defects.[28]

We eliminate mechanisms (1) and (2) as the shunt resistance, R_p, is generally within a factor of two between the various counterions, whereas leakage current and pinholes are typically associated with a reduction of R_p by several orders of magnitude.[5,25] In addition, V_{OC} does not vary significantly with thickness (see Figure S5, Supporting Information), whereas for a pinhole mechanism larger thicknesses would be expected to exhibit higher V_{OC}'s as pinholes are filled. While the lack of variation in R_p also suggests limited mobile ion shunting (3), we performed poling experiments by biasing the devices under ±1 V for 30 min to further investigate this mechanism. Device biasing has been used previously to drive diffusion of counterions toward or away from the heterojunction interface.[27,29] In these studies, devices held under positive bias showed diminished V_{OC}'s and fill factors, whereas those under negative biases showed over 25% increases in V_{OC}. These V_{OC} increases were explained as the result of anion accumulation at the donor–acceptor interface, causing the frontier energy levels of the donor to bend downward and increase the interface gap. Moreover, the variations in V_{OC} were found to strongly depend on counterion size. If these mechanisms were indeed

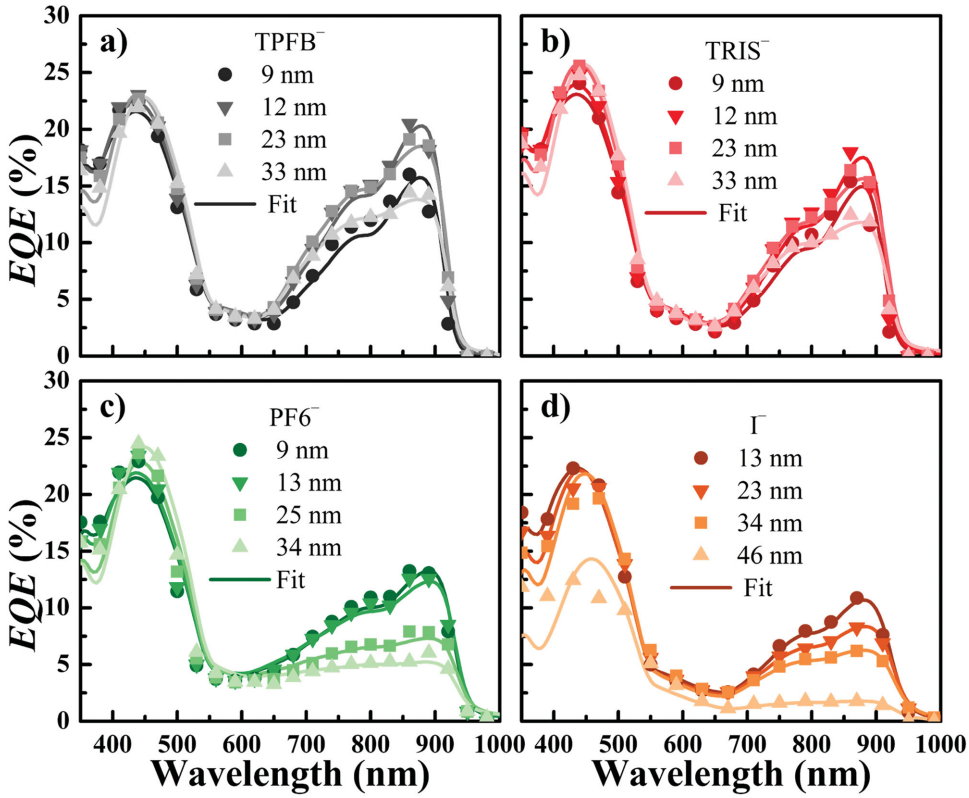

Figure 6. Thickness dependent EQE spectra for a) CyTPFB, b) CyTRIS, c) $CyPF_6$, and d) CyI. Symbols are experimentally measured data and solid lines are fitted EQE used to extract L_D. Measured and fitted EQE for $CySbF_6$ can be found in Figure S3 of the Supporting Information.

significant, one would expect the devices with bulkier anions to show little influence under biasing, as the mobility of these counterions would be considerably reduced and they would be unable to migrate to, or away from, the heterojunction interface during reasonable time scales. However, in our work V_{OC} and FF were not found to vary appreciably (less than 5% for both parameters) in CyI and $CyPF_6$ devices (see Figures S6 and S7, Supporting Information), and therefore is not likely active in these systems, nor is it a plausible mechanism for the changes in voltage and performance. It is possible that the bulkier cation in this work lowers anion mobility, thus significantly increasing the time scale for mobile ion space charge to develop.

Information about recombination and electronic structure can also be extracted from the diode ideality factors (see Table 2). For instance, values of n_{id} between 1 and 2 have been shown to correspond to recombination via tail states.[23] As n_{id} approaches unity, recombination decreases and the concentration of available tail states for charge trapping is reduced. We observe a gradual decrease of n_{id} following the PCE trend, from 2.28 ± 0.05 in CyI devices to 1.28 ± 0.11 in CyTPFB devices. One potential explanation for this trend is variation in bond length alternation (BLA) that has been observed between these counterions. Bouit et al. found that the BLA of a heptamethine cation in the solid state was near zero coordinated with Δ-TRISPHAT⁻, then increased steadily with $TPFB^-$, SbF_6^-, PF_6^-, and I^-.[18] Larger BLAs are also correlated with absorption peak width, and thus likely correspond to a broadened density of states, and an increased Urbach tail energy E_U,[21] around the HOMO and LUMO levels, leading to an increase in tail-sate recombination and n_{id}. The trend in E_U and n_{id} follows the expected BLA trend with the exception of CyTPFB, but the BLA may have only limited value in understanding the optical properties discussed below. The n_{id} also follows the FF trend with the exception of CyTPFB. It seems likely that CyTPFB and CyTRIS are actually within error of each other for both trends, given the relatively large error bar on the n_{id} values for CyTPFB and the proximity of the FFs for each counterion (0.60 and 0.62, respectively).

To differentiate between mechanisms (4) and (5), we perform a counterion mixing experiment by blending $CyPF_6$ (V_{OC} of 0.40 at 1 sun) with CyTPFB (V_{OC} of 0.71 at 1 sun) continuously in planar devices and measuring the variation in performance. A sharp drop in the V_{OC} near one of the purity limits would indicate the presence of dilute defect levels that act as recombination centers,[28] whereas a linear change in V_{OC} would indicate a modulation of the interface energetic gap through fractional averaging of the density of states around different HOMO positions of the two compounds, and therefore shifts in the frontier orbital levels.[30–33] A linear change in V_{OC} could also indicate that the interface gap modulation stems from variation in a dipole shift at the donor–acceptor interface, thus modifying the vacuum and LUMO levels of C_{60} relative to donor salt, but is unlikely in this case due to the dramatic shifts in observed voltages and the lack of variation at the MoO_3/salt interface for different anions. The expected behavior of these

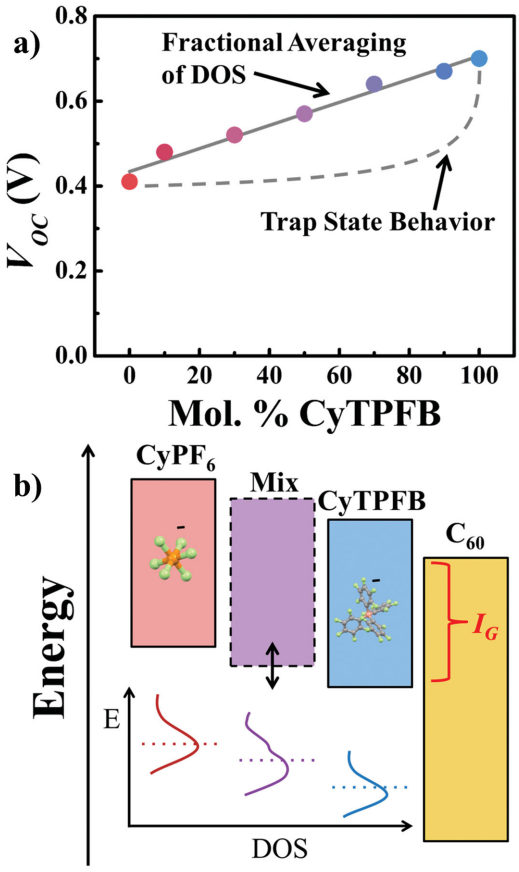

Figure 7. a) V_{OC} as a function of mole percent CyTPFB in blends with $CyPF_6$. The linear trend indicates that increased interface gap via fractional averaging of density of states is the dominant mechanism of V_{OC} enhancement in these devices. The dotted line schematically represents the expected behavior of a dilute mid-gap trap state mechanism for reduction of V_{OC}. b) Schematic representation of the improved energy level alignment between CyTPFB and C_{60}, as well as the tunability of the interface gap via mixtures of $CyPF_6$ and CyTPFB. The inset illustrates the mechanism of density of states (DOS) averaging for shifts in the frontier energy levels and enhanced V_{OC}.

mechanisms is illustrated schematically in **Figure 7**a,b. $CyPF_6$ was chosen for this experiment as PF_6^- and $TPFB^-$ exhibit similar FFs, whereas the I^- anion clearly has multiple mechanistic variables impacting the significantly lower FF. With increasing CyTPFB content, we see a steady linear increase in V_{OC} (Figure 7a) and a significant decline in J_0, which follows the expected behavior for interface gap modulation and HOMO level shifts. We also observe similar linear behavior for mixing with $CySbF_6$ and CyTRIS (see Figure S9, Supporting Information), as well as with other cations. Thus, this identifies the key mechanism responsible for the voltage enhancement and is the first clear evidence in support of an energy level alignment explanation in such systems. This mechanism may also be analogous to similar trends seen in ligand exchange experiments in quantum dot photovoltaics and provides a powerful new tuning parameter for optimizing the HOMO position to balance charge generation with interface recombination and exciton migration dynamics.[34]

To date, there has been no direct characterization of the electronic structure or interface dipoles of polymethines in the solid state. Cyclic voltammetry measurements of polymethine molecules have shown that counterions do not influence the redox properties of the cation in solution; no difference was observed between ClO_4^- and PF_6^-, or between PF_6^- and TRISPHAT$^-$ in larger-gap polymethine derivatives.[16,29] However, it is not clear whether changes in the electronic energy levels in solution are always representative with those in solid-state. Indeed, it has already been shown that the photophysical properties of polymethines vary dramatically between solution and solid state, as aggregation effects begin to dominate their absorption and photoluminescence.[18] As such, it is likely unreasonable to assume that the counterion has no corresponding effect on energy levels and interface gap.

To further confirm mechanism (4), we utilize ultraviolet photoelectron spectroscopy (UPS) to directly measure the frontier energy levels of these polymethines in the solid-state. We find that HOMO levels do indeed shift dramatically based upon the anion. We measure HOMO levels of 4.8 eV for $CyPF_6$ and $CySbF_6$, 4.9 eV for CyTRIS, and 5.2 eV for CyTPFB (see Figure S10 for UPS spectra, Figure S11 for an energy level schematic, and Table S1 for the complete summary of the UPS analysis of the Supporting Information). These UPS measurements directly confirm the interface gap mechanism for voltage modulation, and represent the first direct characterization of the solid-state frontier orbitals of these ionic organic materials.

To put this V_{OC} enhancement in perspective, we compare our results, the V_{OC}'s of state-of-the-art polymethine and small molecule OPVs with the Shockley–Queisser (SQ) and the realistic excitonic voltage limits relative to the optical gaps of each donor material.[7,35] Optical gap and V_{OC} data for the best reported ionic cyanine photovoltaics are compiled in Table S2 of the Supporting Information and are plotted in **Figure 8**. The majority of reported cyanine OPVs have V_{OC}'s <40%–60% of the excitonic limit. At 82% of the excitonic voltage limit, CyTPFB shows the highest relative reported V_{OC} for a cyanine-based

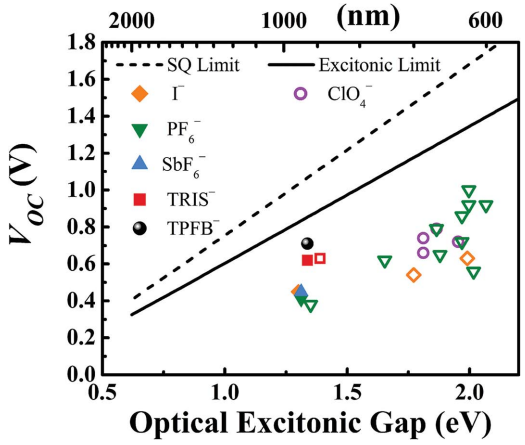

Figure 8. V_{OC} as a function of optical gap for various cyanine–C_{60} heterojunction solar cells. The dotted line is the theoretical Shockley–Queisser voltage limit and the solid line is the semiempirical excitonic voltage limit for organic photovoltaics.[7,35]

photovoltaic. Indeed, to the best of our knowledge, this is the highest reported V_{OC} for any small molecule OPV with photoresponse past 900 nm.[7]

3.2. Effect of the Counterion on Photophysical Properties

The observed reduction in peak width, Figure 3a, can likely be attributed to a combination of the increased separation (and corresponding reduced aggregation and interaction) between Cy^+ cations and the decreased polarization of the Cy^+ cation seen in crystalline solids of these salts.[18] Both of these effects would result in a decreased distribution of available states for absorption. The slightly larger breadth of the CyTPFB peak relative to the CyTRIS peak is consistent with the findings of Bouit et al. that Δ-TRISPHAT$^-$ induces less polarization and bond length alternation than TPFB$^-$ and harder counterions in other core polymethine derivatives.[18] While the narrowing of the peaks does correspond to a slight decrease in the optical gap of ≈0.03 eV, this is clearly insufficient to explain a 0.3 V increase in V_{OC}. Nonetheless, peak narrowing has the advantage of increasing average visible transmittance and color rendering index for transparent photovoltaic applications. The long wavelength cut-off of photopic response is at ≈675 nm,[11] and as can be seen in Figure 3a, the CyTPFB and CyTRIS have considerably less overlap with the photopic response curve than the other anions, CyI, $CyPF_6$, and $CySbF_6$. Narrowing could also have the benefit of decreasing competitive absorption with other NIR donors in multijunction transparent photovoltaics for enhanced performance.

3.3. Exciton Diffusion Length Enhancement

The mechanism behind the improvement in L_D, Figure 4b, is not yet entirely clear. The enhancement could be due to the increased spacing between donor molecules and a concomitant increase in Förster transfer.[36,37] However, because we observe no photoluminescence from these materials (implying a quantum yield for luminescence <0.1%, our detection limit), Förster transfer is less likely to be the dominant exciton transport mechanism. The optical scaling suggested by a Förster mechanism ($L_D \propto n^{-2}$, where n is the refractive index) may account for approximately half of the L_D enhancement, and is possibly offset by changes in luminescence quantum yield that are below our detection level.[37] The alternative mechanism of Dexter transfer could be the dominant mechanism of exciton transfer in this case. However, the spacing dependence of this mechanism is at odds with the observed trend, where larger spacings should lead to lower orbital overlap and decreased diffusions lengths. While we do not have a clear explanation for the diffusion length trend that is observed, it is interesting to note that it is not clearly correlated to any one particular parameter such as ion size (nor is the V_{OC}, see Figure 4b), and there is a demonstrably sensitive competition of effects as seen between the variations of I$^-$ with TPFB$^-$, and even more interestingly between TRIS$^-$ and TPFB$^-$. Future studies could explore the radius, ordering, and shape of aromatic counterions further to study the effect of cation spacing on photophysical and electronic transport properties.

The selection of counterions for new polymethine materials will clearly involve an intentional balancing of V_{OC} and J_{SC}, by tuning the energy levels to optimize for the combination of both the largest interface gap and the highest exciton dissociation efficiency. In addition, the influence of the counterion on exciton diffusion length and optical properties should be sensitively considered as a key optimization variable for this class of photovoltaic materials.

4. Conclusion

We have systematically demonstrated a new series of organic polymethine salts in photovoltaic devices that exhibit open-circuit voltage enhancement from 0.41 to 0.71 V for selective NIR harvesting past 900 nm via anion exchange without significantly altering bandgaps. Relative to the optical excitonic gap of this molecule, this is the highest reported V_{OC} for a cyanine-based photovoltaic, nearing the excitonic photovoltaic voltage limit and the highest reported V_{OC} for any small molecule OPV with photoresponse past 900 nm. Anion exchange also results in a near doubling of peak NIR EQE from 11% to 21% at 880 nm. We attribute these improvements to the tunability of the interface energy gap with anion selection, as well as enhancements in exciton diffusion lengths. We show that steric hindrance alone cannot be used as an optimization design principle for anion modification, and further, that anion selection and alloying can be utilized as a key optimization parameter to control the frontier orbital levels and optoelectronic properties in these devices. This study suggests key strategies for improving organic salt based photovoltaics through variation of bulky counterions that is likely applicable to a diverse range of cyanine and organic salt active layers. The fine energy level control afforded by these strategies will allow for the rapid realization of novel donor–acceptor pairings with efficient response even deeper into the NIR with maximal voltages. This work offers a promising path toward achieving high voltage near-infrared absorbing organic photovoltaics and highly efficient transparent photovoltaics.

5. Experimental Section

Materials and Synthesis: 2-[2-[2-chloro-3-[2-(1,3-dihydro-3,3-dimethyl-1-ethyl-2H-benz[e]indol-2-ylidene)ethylidene]-1-cylohexen-1-yl]-ethenyl]-3,3-dimethyl-1-ethyl-1H-benz[e]indolium iodide (CyI, American Dye Source) was filtered through a plug of silica with a 5:1 DCM:MeOH solvent mixture to remove impurities. Lithium tetrakis(pentafluorophenyl)borate ethyl etherate, $NaPF_6$ (98%), and $AgSbF_6$ (98%) (Sigma-Aldrich) were used as received. Δ-tris(tetrachloro-1,2-benzenediolato)phosphate(V) (Δ-TRISPHAT) tetrabutylammonium salt (98.5%) (Santa Cruz Biotechnology), C_{60} (99.9%) (MER Corp.), bathocuproine (BCP) (Luminescence Technology, Inc.), and MoO_3 (99.9995%) (Alfa Aesar) were all used as received. All exchanges followed similar procedures described previously,[8,9] except for $CySbF_6$, which was exchanged via a precipitation reaction with $AgSbF_6$ in DCM. The solution of CyI and $AgSbF_6$ was stirred for 3 h at room temperature before washing over filter paper with DCM. All exchange products were filtered through a plug of silica with DCM as an eluent, which allowed for the more polar remnant CyI to be easily removed. Purity was verified using Mass Spectrometry (Waters Xevo G2-XS quadrupole time-of-flight) with direct injection.

Solutions with concentrations from (5–500) $\times$ 10^{-9} M were prepared of $CyPF_6$ and CyTPFB, as well as K-TPFB, CyI, and $NaPF_6$ to generate standard reference curves. In testing the purity of $CyPF_6$ and CyTPFB, all solutions were prepared in 50%/50% acetonitrile (ACN)/H_2O and 100% ACN, respectively for each material. CyTPFB was shown to have <1.0 mol% iodide content and $CyPF_6$ was shown to have <2 mol% iodide content. See Figures S12–S15 and Tables S3 and S4 of the Supporting Information for details. Electron dispersive spectroscopy (EDS) was also used to verify successful exchange of the counterion, indicated by reduction of the iodine Lα peak and the appearance of P and/or F peaks in the EDS spectra. The resulting iodide impurities were also shown to be better than the detection limit of the EDS (<1%–2%).

Device Fabrication and Testing: Glass substrates prepatterned with 100 nm of ITO were cleaned by sequential sonication in soap, deionized water, and acetone for 4 min each, followed by boiling in isopropanol for 5 min and oxygen plasma treatment for 5 min. All devices were fabricated with an active area of 5.2 mm^2. Compounds (1)–(4) were spin-coated for 5 s at 600 rpm followed by 20 s at 2000 rpm from chlorobenzene solutions of varying concentrations. Compound (5) was dissolved in a 3:1 CB:DCM solution due to limited solubility in CB. To eliminate the effect of the solvent, a control experiment was performed with various solvents showing that there was negligible performance variation between devices fabricated with CB alone versus CB:DCM (3:1) mixture for any of the five compounds, see Figure S16 of the Supporting Information. All other layers were deposited at 0.1 nm/s via vacuum thermal evaporation with a pressure below 3×10^{-6} Torr. Film thicknesses were determined using variable-angle spectroscopic ellipsometry. The device structure for opaque devices was: MoO_3 (10 nm)/Cy (*x* nm)/C_{60} (40 nm)/BCP (7.5 nm)/Ag (80 nm). The device structure for transparent devices was: MoO_3 (10 nm)/Cy (*x* nm)/C_{60} (40 nm)/BCP (7.5 nm)/Ag (2 nm)/MoO_3 (100 nm)/ITO (100 nm). Current density (*J*) was measured as a function of voltage (*V*) under dark conditions and AM 1.5G solar simulation (xenon arc lamp) in air, where the intensity was measured using a NREL-calibrated Si reference cell with KG5 filter. *J*–*V* characteristics were averaged over at least 12 devices fabricated in three independent device sets. EQE measurements were calibrated using a Newport calibrated Si detector.

Optical and Electronic Characterization and Modeling: Specular transmittance of films and device stacks were measured using a dual-beam Lambda 800 UV/vis spectrometer in the transmission mode without the use of a reference sample. Average visible transmittance was calculated by weighting the transmission spectra with the solar spectrum and the photopic response of the human eye.[1] Optical gaps were approximated as the long-wavelength cut-off at 10% of the peak height and were extracted from EQE data when possible, and were otherwise taken from absorbance or optical constant data. Optical constants for optical modeling were determined with variable angle ellipsometry (see Figure S17, Supporting Information). Exciton diffusion lengths were extracted from EQE data using transfer matrix optical modeling and least squares regression across all thickness sets.

UPS data were recorded with a He lamp emitting at 21.2 eV (He I radiation) on salt films grown on ITO/MoO_3 that were loaded without exposure to air. For energy level drawings, the LUMO positions were estimated by adding the optical gap (1.3 eV).[34]

Supporting Information

Supporting Information is available from the Wiley Online Library or from the author.

Acknowledgements

The authors would like to thank Prof. Sophia Y. Lunt and the MSU Mass Spectrometry and Metabolomics Core. The authors also thank Prof. Annick Anctil for helpful discussions. Financial support for this work was provided in part by the National Science Foundation (CAREER Award No. CBET-1254662) and (IIP-1431010), and a DuPont Young Professor Award.

Received: August 18, 2015
Published online: October 30, 2015

[1] R. R. Lunt, *Appl. Phys. Lett.* **2012**, *101*, 043902.
[2] J. D. Zimmerman, V. V. Diev, K. Hanson, R. R. Lunt, E. K. Yu, M. E. Thompson, S. R. Forrest, *Adv. Mater.* **2010**, *22*, 2780.
[3] M. S. Arnold, J. D. Zimmerman, C. K. Renshaw, X. Xu, R. R. Lunt, C. M. Austin, S. R. Forrest, *Nano Lett.* **2009**, *9*, 3354.
[4] M. J. Shea, M. S. Arnold, *Appl. Phys. Lett.* **2013**, *102*, 243101.
[5] N. Li, B. E. Lassiter, R. R. Lunt, G. Wei, S. R. Forrest, *Appl. Phys. Lett.* **2009**, *94*, 023307.
[6] H.-S. Shim, H. J. Kim, J. W. Kim, S.-Y. Kim, W.-I. Jeong, T.-M. Kim, J.-J. Kim, *J. Mater. Chem.* **2012**, *22*, 9077.
[7] R. R. Lunt, T. P. Osedach, P. R. Brown, J. A. Rowehl, V. Bulović, *Adv. Mater.* **2011**, *23*, 5712.
[8] R. R. Lunt, V. Bulovic, *Appl. Phys. Lett.* **2011**, *98*, 113305.
[9] C.-C. Chen, L. Dou, R. Zhu, C.-H. Chung, T.-B. Song, Y. B. Zheng, S. Hawks, G. Li, P. S. Weiss, Y. Yang, *ACS Nano* **2012**, *6*, 7185.
[10] T. P. Osedach, A. Iacchetti, R. R. Lunt, T. L. Andrew, P. R. Brown, G. M. Akselrod, V. Bulović, *Appl. Phys. Lett.* **2012**, *101*, 113303.
[11] J. M. Hales, J. Matichak, S. Barlow, S. Ohira, K. Yesudas, J.-L. Brédas, J. W. Perry, S. R. Marder, *Science* **2010**, *327*, 1485.
[12] Y. Zhao, G. A. Meek, B. G. Levine, R. R. Lunt, *Adv. Opt. Mater.* **2014**, *2*, 606.
[13] B. Fan, F. A. de Castro, J. Heier, R. Hany, F. Nüesch, *Org. Electron.* **2010**, *11*, 583.
[14] R. Hany, B. Fan, F. A. de Castro, J. Heier, W. Kylberg, F. Nüesch, *Prog. Photovolt. Res. Appl.* **2011**, *19*, 851.
[15] H. Zhang, G. Wicht, C. Gretener, M. Nagel, F. Nüesch, Y. Romanyuk, J.-N. Tisserant, R. Hany, *Sol. Energy Mater. Sol. Cells* **2013**, *118*, 157.
[16] A. C. Véron, H. Zhang, A. Linden, F. Nüesch, J. Heier, R. Hany, T. Geiger, *Org. Lett.* **2014**, *16*, 1044.
[17] P.-A. Bouit, C. Aronica, L. Guy, A. Martinez, C. Andraud, O. Maury, *Org. Biomol. Chem.* **2009**, *7*, 3086.
[18] P.-A. Bouit, C. Aronica, L. Toupet, B. Le Guennic, C. Andraud, O. Maury, *J. Am. Chem. Soc.* **2010**, *132*, 4328.
[19] O. Malinkiewicz, T. Grancha, A. Molina-Ontoria, A. Soriano, H. Brine, H. J. Bolink, *Adv. Energy Mater.* **2013**, *3*, 472.
[20] B. P. Rand, D. P. Burk, S. R. Forrest, *Phys. Rev. B* **2007**, *75*, 115327.
[21] A. Foertig, J. Rauh, V. Dyakonov, C. Deibel, *Phys. Rev. B* **2012**, *86*, 115302.
[22] L. A. A. Pettersson, L. S. Roman, O. Inganäs, *J. Appl. Phys.* **1999**, *86*, 487.
[23] T. Kirchartz, B. E. Pieters, J. Kirkpatrick, U. Rau, J. Nelson, *Phys. Rev. B* **2011**, *83*, 115209.
[24] O. Malinkiewicz, M. Lenes, H. Brine, H. J. Bolink, *RSC Adv.* **2012**, *2*, 3335.
[25] O. Kunz, J. Wong, J. Janssens, J. Bauer, O. Breitenstein, A. g. Aberle, *Prog. Photovolt. Res. Appl.* **2009**, *17*, 35.
[26] M. T. Lloyd, A. C. Mayer, A. S. Tayi, A. M. Bowen, T. G. Kasen, D. J. Herman, D. A. Mourey, J. E. Anthony, G. G. Malliaras, *Org. Electron.* **2006**, *7*, 243.
[27] M. Lenes, H. J. Bolink, *ACS Appl. Mater. Interfaces* **2010**, *2*, 3664.
[28] R. A. Street, P. P. Khlyabich, A. E. Rudenko, B. C. Thompson, *J. Phys. Chem. C* **2014**, *118*, 26569.

[29] H. Benmansour, F. A. Castro, M. Nagel, J. Heier, R. Hany, F. Nüesch, *Chim. Int. J. Chem.* **2007**, *61*, 787.
[30] P. P. Khlyabich, B. Burkhart, B. C. Thompson, *J. Am. Chem. Soc.* **2011**, *133*, 14534.
[31] P. P. Khlyabich, B. Burkhart, B. C. Thompson, *J. Am. Chem. Soc.* **2012**, *134*, 9074.
[32] T. Goh, J.-S. Huang, E. A. Bielinski, B. A. Thompson, S. Tomasulo, M. L. Lee, M. Y. Sfeir, N. Hazari, A. D. Taylor, *ACS Photonics* **2015**, *2*, 86.
[33] R. A. Street, D. Davies, P. P. Khlyabich, B. Burkhart, B. C. Thompson, *J. Am. Chem. Soc.* **2013**, *135*, 986.
[34] P. R. Brown, D. Kim, R. R. Lunt, N. Zhao, M. G. Bawendi, J. C. Grossman, V. Bulović, *ACS Nano* **2014**, *8*, 5863.
[35] W. Shockley, H. J. Queisser, *J. Appl. Phys.* **1961**, *32*, 510.
[36] T. K. Mullenbach, K. A. McGarry, W. A. Luhman, C. J. Douglas, R. J. Holmes, *Adv. Mater.* **2013**, *25*, 3689.
[37] R. R. Lunt, N. C. Giebink, A. A. Belak, J. B. Benziger, S. R. Forrest, *J. Appl. Phys.* **2009**, *105*, 053711.